

Alfredo E. Varela<sup>1</sup> and Marianela Suárez

## FEMLAB Simulation of Thermoplastics Injection-Molding

**Abstract** The thermoplastics injection-molding process has become one of the most important polymer processing operations in the production of molded parts with geometric complexity and high precision. Modeling and computer simulation of this process is not an easy task. Commercial computer packages have been designed for the simulation of the injection molding process. These programs allow the determination of the effects of operational conditions on the quality of molded parts. However, they require a high demand of computing time, and their costs restrict its use to companies with financial capacity. FEMLAB offers graphical and computational tools that can be implemented for analysis and design of a variety of cavity geometries and visualization of some process characteristics.

### 1 Introduction

Figure 1 shows a schematic of a reciprocating injection-molding machine and the rectangular cavity. The molding is a cyclic process, where the polymer melt is forced by shearing and heating into the small cavity placed between cooling plates. In the cavity, the molten polymer solidifies after cooling below its melt temperature. Then, the molded part is expelled by one of the plates, and the cycle is repeated.

The cavity process is divided into three stages: filling, packing and cooling. In the filling stage the melt occupies the cavity volume. In the packing stage, additional material is forced into the cavity to compensate for an increasing polymer density during the cooling stage.

This work is intended to present a preliminary method for the simulation of polystyrene injection-molding in a rectangular cavity using FEMLAB 3.1. This approach is based on published mathematical models in partial differential equations of mass, energy and momentum balance, as well as the constitutive equations of viscosity, thermal conductivity and specific heat.

**Keywords** Thermoplastics, injection molding, FEMLAB 3.1.

<sup>1</sup> Universidad de Carabobo, Facultad de Ingeniería. Valencia, Venezuela 2001. E-mail: [avarela@uc.edu.ve](mailto:avarela@uc.edu.ve)

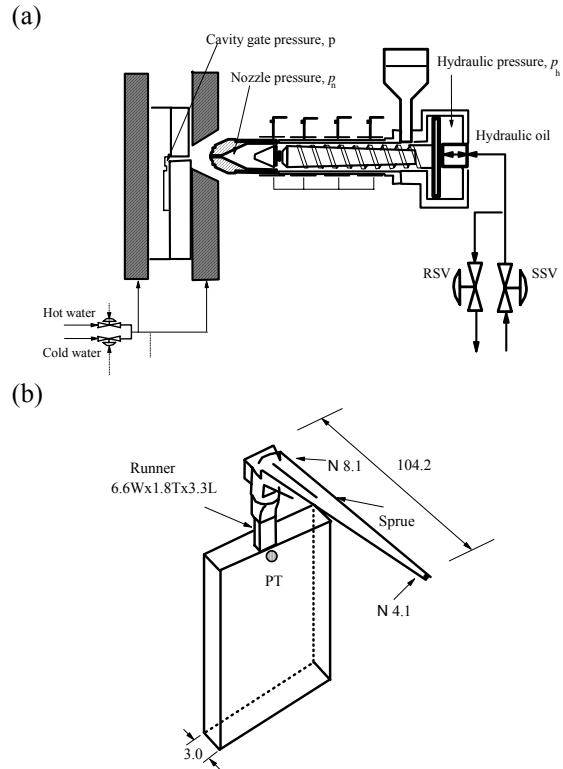


**Fig. 1** Schematic of an (a) injection molding machine and (b) the rectangular cavity.

Figure 2 presents the typical variation of cavity and nozzle pressure in a cycle. These pressures were measured by using two pressure transducers, one placed at the nozzle and the other flush with the cavity surface near the gate. The cavity gate pressure increases rapidly during the filling and packing stages, and then start to drop when the gate freezes, until the end of cooling.

### 2 Model Definition

A number of mathematical models have been proposed for the cavity process simulation in thermoplastics injection-molding. Hieber and Shen [1] presented a model for the prediction of pressure and temperature during the filling of thin cavities using the Hele-Shaw flow model. In this model, for a rectangular cavity such as the schematic shown in Figure 1b, the velocity is considered to be integrated

by components  $u_x$  and  $u_y$  that depend on the coordinate  $z$ , the gapwise coordinate. Thus, the  $x$  and  $y$  components of the equation of motion are written as

$$\frac{\partial}{\partial z} \left( \eta \frac{\partial u_x}{\partial z} \right) - \frac{\partial p}{\partial x} = 0, \quad \frac{\partial}{\partial z} \left( \eta \frac{\partial u_y}{\partial z} \right) - \frac{\partial p}{\partial y} = 0 \quad (1)$$

and the continuity and energy equations are given by

$$\frac{\partial}{\partial z} (b \langle u_x \rangle) - \frac{\partial}{\partial x} (b \langle u_y \rangle) = 0, \quad (2)$$

$$\rho C_p \frac{\partial T}{\partial t} - \left[ \frac{\partial}{\partial x} \left( k \frac{\partial T}{\partial x} \right) + \frac{\partial}{\partial y} \left( k \frac{\partial T}{\partial y} \right) + \frac{\partial}{\partial z} \left( k \frac{\partial T}{\partial z} \right) \right] + \rho C_p \left( u_x \frac{\partial T}{\partial x} + u_y \frac{\partial T}{\partial y} \right) = \eta \dot{\gamma}^2 \quad (3)$$

where  $\eta$  is the polymer viscosity.

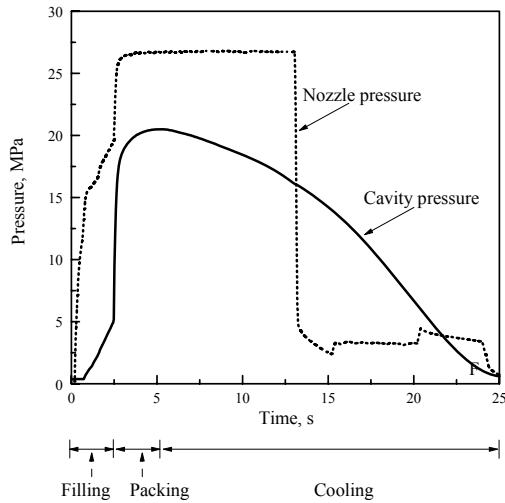


**Fig. 2** Variation of the cavity-gate pressure with time in a cycle.

The following equations are used for calculation of polymer properties. A Cross-type model [2a] is used for the viscosity

$$\eta = \eta_o \left[ 1 + \left( \frac{\eta_o}{\dot{\gamma} \tau^*} \right)^{1-n} \right]^{-1}, \quad (4)$$

$$\dot{\gamma} = \sqrt{(\partial u_x / \partial z)^2 + (\partial u_y / \partial z)^2}$$

and an Arrhenius-type model is recommended for  $\eta_o$

$$\eta_o = B \exp \left( \frac{T_b}{T} \right) \exp(\beta p). \quad (5)$$

The density  $\rho$  is obtained from the Tait equation of state for the specific volume  $v$  of an amorphous polymer

$$v = v_o \left[ 1 - C \log \left( 1 + \frac{p}{B} \right) \right]. \quad (6)$$

where  $C = 0.0894$ ,  $v_o$  and  $B(T)$  are represented [2a] by

$$v_o = \begin{cases} b_{1,i} + b_{2,i} \bar{T} & \text{if } T > T_i \\ b_{1,s} + b_{2,s} \bar{T} & \text{if } T < T_i \end{cases}, \quad (6a)$$

$$B(T) = \begin{cases} b_{3,i} \exp(-b_{4,i} \bar{T}) & \text{if } T > T_i \\ b_{3,s} \exp(-b_{4,s} \bar{T}) & \text{if } T < T_i \end{cases}$$

where  $\bar{T} = T - b_5$ ,  $T_i(p) = b_5 + b_6 p$ . For the specific heat,  $C_p$ , and thermal conductivity,  $k$ , the following equations were suggested

$$C_p = c_1 + c_2 \bar{T} + c_3 \tanh(c_4 \bar{T}), \quad (7)$$

$$k = \lambda_1 + \lambda_2 \bar{T} + \lambda_3 \tanh(\lambda_4 \bar{T})$$

where  $\bar{T} = T - c_5$ ,  $\bar{T} = T - \lambda_5$ .

Integration of Eqs (1) across the cavity thickness conducts to the fluidity term given as

$$S = \int_0^b \frac{z^2 dz}{\eta}. \quad (8)$$

Substituting Eq. (8) into Eq. (1) gives

$$\frac{\partial}{\partial x} \left( S \frac{\partial p}{\partial x} \right) + \frac{\partial}{\partial y} \left( S \frac{\partial p}{\partial y} \right) = 0 \quad (9)$$

Figure 3 depicts the axis coordinates and geometries defined in order to solve Equations (3) and (9). Appropriate boundary conditions are defined as follows. At the cavity entry ( $x = 0$ ,  $0 \leq y \leq g_w$ ,  $0 \leq z \leq g_h$ ):  $T = T_e$ ,  $p = p_o$ , where  $g_w$  and  $g_h$  are the gate width and height for the rectangular gate. At the cavity walls:  $T = T_w$ ,  $\partial p / \partial n = 0$ , and at the mid-cavity gapwise plane ( $y = 0$ ):  $\partial T / \partial z = 0$ ,  $\partial p / \partial x = 0$ .

### 3 Modeling Using FEMLAB

#### 3.1 Geometry Modeling

A 2D (**Geom1**) and 3D (**Geom3**) geometries were created for the solution of the temperature and pressure equations in the mid-cavity, as illustrated in Figure 3, by drawing a rectangle with representative dimensions,  $\hat{L}_c = 3$ ,  $\hat{A}_c = 1$ ,  $\hat{b} = 0.1$  for the cavity, and  $\hat{g}_w = \hat{A}_c$ ,  $\hat{g}_h = \hat{g}_w \hat{b} / \hat{b}$  for the gate. The mid-cavity is modeled by creating first an intermediate 2D geometry (**Geom2**) with two solid rectangles in the  $y$ - $z$  plane with dimensions  $y = \hat{A}_c$ ,  $z = \hat{b}$  for the cavity, and  $y = \hat{g}_w$ ,  $z = \hat{g}_h$  for the gate. In order to create the 3D geometry (**Geom3**), the cavity base rectangle is extruded a distance equivalent to the representative

cavity length ( $x = \hat{L}_c$ ), and then the gate rectangle is embedded into the 3D geometry.

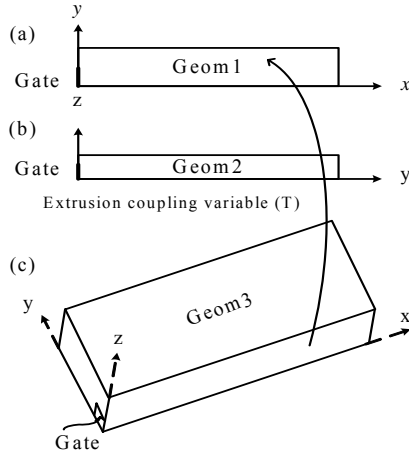


Fig. 3 Geometry modeling.

### 3.2 Physics Settings

The equation system considered is in the FEMLAB PDE coefficient form [3] as

$$d_a \frac{\partial u}{\partial t} - \nabla \cdot (c \nabla u + \alpha u - \gamma) + \beta \cdot \nabla u + au = f \quad (10)$$

where

$$u = \begin{bmatrix} p \\ T \end{bmatrix}, d_a = \begin{bmatrix} 0 \\ \rho C_p \end{bmatrix}, c = \begin{bmatrix} S \\ \hat{ } \\ k \end{bmatrix} \quad (11)$$

$$\beta = \begin{bmatrix} 0 & 0 \\ \rho C_p u_x / scale_x^2 & \rho C_p u_y / scale_y^2 & 0 \end{bmatrix}, f = \begin{bmatrix} 0 \\ \eta \gamma^2 \end{bmatrix}$$

$\alpha = 0, \gamma = 0, a = 0$ . The associated FEMLAB boundary conditions are written as

$$hu = r, n \cdot (c \nabla u + \alpha u - \gamma) + qu = g - h^T \mu \quad (12).$$

For the pressure on the 2D (Geom1), as seen in Figure 3a, Neumann boundary conditions ( $n \cdot (c \nabla p) = 0$ ) are considered along edge  $y = 0$ , as well as on edge  $x = 0, \hat{A}_c \geq y \geq \hat{g}_w$  that represents the cavity wall near the gate. Edges at  $x = \hat{L}_c$  and  $y = \hat{A}_c$  are assumed to be at Dirichlet conditions ( $h = 1, r = p$ ). In addition, the gate is also assumed to be at a Dirichlet-type boundary condition  $h = 1, r = p_0$ . The gate pressure  $p_0$  was shown in Figure 2, and fits the empirical equation

$$p_0 = \begin{cases} \alpha t, & t_{fill} \geq t \geq 0 \\ p_{ef} + (p_p - p_{ef})(1 - \exp(-t/\tau)), & t_{pack} \geq t \geq t_{fill} \end{cases} \quad (13)$$

where  $t_{fill} = 2.5$  s,  $t_{pack} = 2.5$  s; these are the time intervals for the filling and packing stages. Other parameters are  $\alpha = 5.19$  MPa/s,  $p_{ef} = 5.19$  MPa,  $p_p = 22.06$  MPa,  $\tau = 0.16$  s.

Respect to geometry in 3D (Geom3) for temperature, Neumann condition ( $n \cdot (c \nabla T) = 0$ ) is considered on planes  $x-z$ , which is symmetric respect to coordinate  $y$ , and Dirichlet conditions at the cavity walls ( $h = 1, r = T_{mold}$ ), at the melt front ( $h = 1, r = T$ ), and at the gate ( $h = 1, r = T_0$ ).  $T_0$  is the polymer temperature entering the gate.

Eqn. (10) constitutes a differential-algebraic system (DAE [3]) which involves singular mass matrices during the finite element computations. Therefore, a procedure was implemented where the time changed iteratively, saving the solution of one time for the next time interval. These equations are connected because  $k$  and  $S$  depend indirectly on  $u_x, u_y, T$ , and  $p$ . Then, extrusion coupling variables are employed to make the temperature from the 3D-geometry (Geom1) available on the 2D-geometry (Geom1). Figure 4 provides a flow diagram for the numerical implementation using a script file running under FEMLAB 3.1-MATALAB environment.

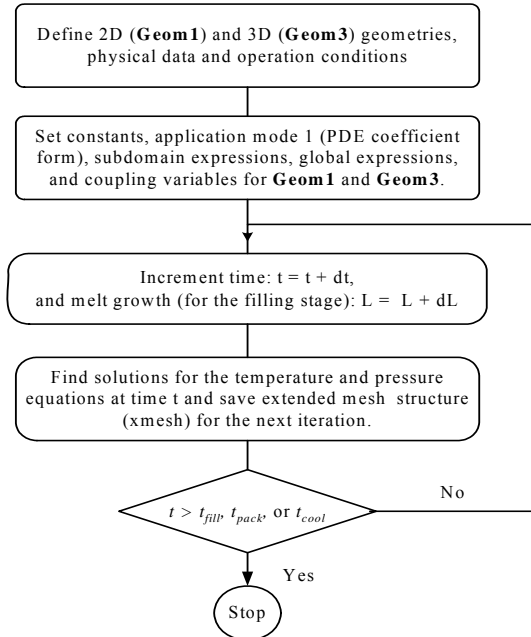


Fig. 4 Flow diagram for the solution during the filling, packing and cooling stages.

#### 4 Results and Discussion

In order to run the scrip file, data is required as the cavity dimensions, the melt temperature, variations of cavity gate pressure with time, and the time intervals for the filling, packing and cooling stages. The cavity polymer velocities are estimated as the cavity length and cavity width divided by the filling time ( $u_x = L_c/t_{fill}$ ,  $u_y = A_c/t_{fill}$ ). Table 1 lists the polystyrene properties [2b] required in Eqs. (4 - 7).

Figure 5 presents the cavity pressure distribution at the end of the filling and packing stages. The pressure gradients are higher during the filling stage than in the packing stage, which corresponds with experimental observations. Figure 6 illustrates the variations of temperature fields at the end of filling and packing. As seen in Figure 6a, temperatures near the ends are close to the temperature of the melt entering the cavity ( $T_0 = 493$  K), while they approach to the wall temperature ( $T_{mold} = 313$  K) near the mid-cavity-plane. The opposite occurs in the packing stage as shown in Figure 6b. This effect is attributed to viscous heating effects, it can be also inferred from the surface temperature plot shown in Figure 7.

Table 1. Parameters for estimating polystyrene properties [2b].

Viscosity	Specific volume
$n = 0.274$	$b11 = 9.88e-4 \text{ m}^3/\text{kg}$
$\tau^* = 2.50e4 \text{ Pa}$	$b21 = 6.10e-7 \text{ m}^3/(\text{kg}\cdot^\circ\text{C})$
$B = 3.04 \text{ e-9 Pa}\cdot\text{s}$	$b31 = 115 \text{ MPa}$
$T_b = 13300 \text{ K}$	$b41 = 3.66e-3 \text{ }^\circ\text{C}^{-1}$
$\beta = 3.5e-8 \text{ Pa}^{-1}$	$b1s = 9.88e-4 \text{ m}^3/\text{kg}$
	$b2s = 1.49e-7 \text{ m}^3/(\text{kg}\cdot^\circ\text{C})$
	$b3s = 238 \text{ MPa}$
	$b4s = 2.10e-3 \text{ }^\circ\text{C}^{-1}$
	$b5s = 112 \text{ }^\circ\text{C}$
	$b6s = 7.8e-7 \text{ }^\circ\text{C}\cdot\text{Pa}^{-1}$
Specific heat	Thermal conductivity
$c1 = 1550 \text{ J}/(\text{kg }^\circ\text{C})$	$\lambda_1 = 0.149 \text{ W}/(\text{m }^\circ\text{C})$
$c2 = 2.99 \text{ J}/(\text{kg }^\circ\text{C}^2)$	$\lambda_2 = 1.63e-4 \text{ W}/(\text{m}^\circ \text{C}^2)$
$c3 = 174 \text{ J}/(\text{kg }^\circ\text{C})$	$\lambda_3 = 0$
$c4 = 6.68e-2 \text{ }^\circ\text{C}$	$\lambda_4 = 0$
$c5 = 79.6 \text{ }^\circ\text{C}$	$\lambda_5 = 100 \text{ }^\circ\text{C}$

#### 5 Conclusion

This preliminary work has presented a method capable of determining pressure and temperature distributions in a rectangular cavity. Future work shall include the following: 1) Use of extrusion coupling variables for pressure and temperature between 2D and

3D geometries, 2) Improvement in the models by using a time varying model and a 3D geometry for the cavity pressure, 3) Inclusion in the results of process variables such as the melt flow front and interface positions during the filling stage, and 4) Validation of the models.

#### Acknowledgement

This work has been supported by the Science and Humanistic Development Council of the University of Carabobo (Project CDCH-1951-04), Valencia, Venezuela.

#### References

1. Hieber, C.A. and S. F. Shen. A Finite Element/Finite Difference Simulation of the Injection Molding Filling Process. *J. Non-Newtonian Fluid Mech.*, **7**, 1-32 (1980).
- 2a. Chiang, H., Hieber, C. and Wang, K.T. A unified simulation of the filling and postfilling stages in injection molding. Part I: Formulation”, *Polymer Engineering and Science*, 31(2), USA, pp. 116-124 (1991).
- 2b. Chiang, H., Hieber, C. and Wang, K.T. A unified simulation of the filling and postfilling stages in injection molding. Part II: Experimental verification, *Polymer Engineering and Science*, 31(2), USA, pp. 125-139 (1991).
3. Femlab 3. Chemical Eng. Module, Model Library. Comsol AB, p 203 (2004).
4. Femlab 3. User's Guide. Comsol AB., p 234 (2004).

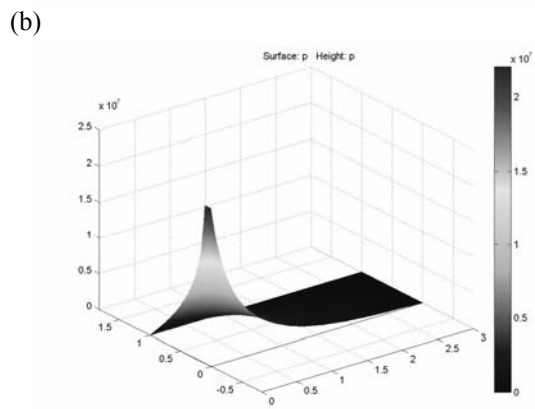
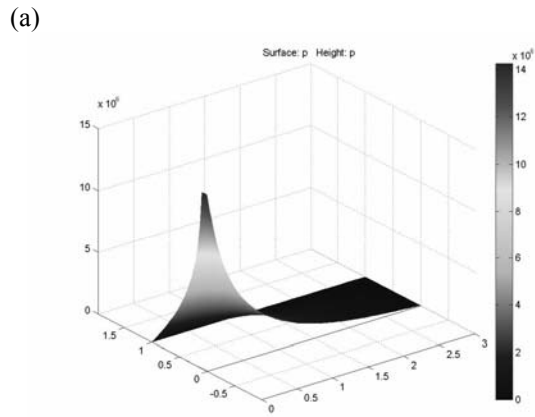


**Fig. 5** Variation of the cavity pressure at the end of the (a) filling and (b) packing stages.

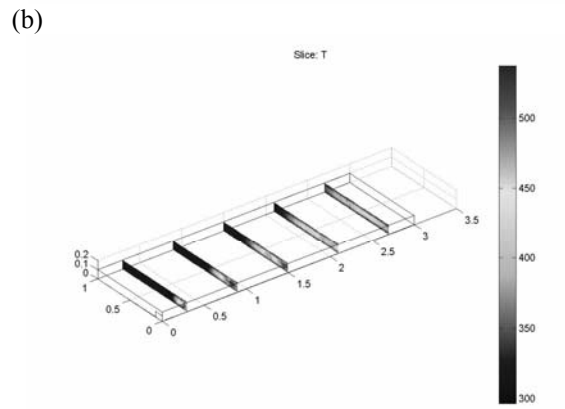
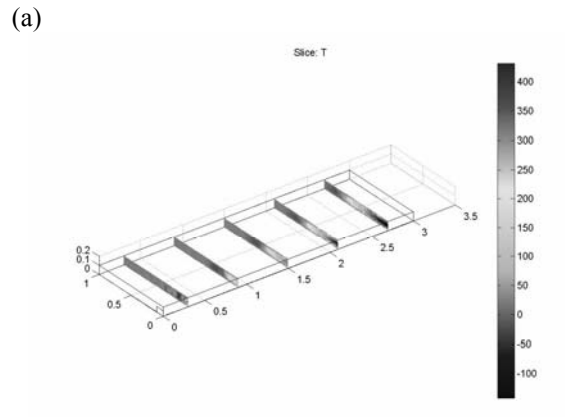


**Fig. 6** Temperature profiles at the end of the (a) filling and (b) packing stages.

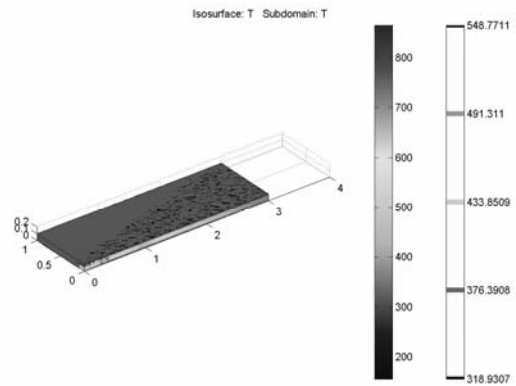


**Fig. 7** Surface plot of temperature distributions at the end of the (a) filling and (b) packing stages.